JOURNAL OF CATALYSIS 117, 170–187 (1989)

# The Genesis of Carbon-Supported Fe–Mn and K–Fe–Mn Catalysts from Stoichiometric Metal Carbonyl Clusters

## I. Characterization by Diffuse Reflectance Infrared Fourier Transform Spectroscopy (DRIFTS)

JEREMY J. VENTER, ANDY CHEN, AND M. ALBERT VANNICE[1]

*Department of Chemical Engineering, Pennsylvania State University, University Park, Pennsylvania 16802*

Received September 13, 1988; revised December 30, 1988

The thermal decomposition of $Fe_3(CO)_{12}$, $NEt_4[Fe_2Mn(CO)_{12}]$, $Mn_2(CO)_{10}$, $K[HFe_3(CO)_{11}]$, and $K[Fe_2Mn(CO)_{12}]$ has been studied for the first time by dispersing these clusters on an oxygen-free carbon surface and monitoring their behavior by diffuse reflectance Fourier transform infrared spectroscopy (DRIFTS). The $Fe_3(CO)_{12}$ decomposed to $Fe(CO)_5$ in either He or $H_2$, while $Mn_2(CO)_{10}$ decarbonylated without the formation of any stable intermediate clusters in either gas. The $NEt_4[Fe_2Mn(CO)_{12}]$ clusters decomposed with no formation of other stable carbonyl products in He, but in $H_2$ they formed $Mn_2(CO)_{10}$ and $[HFe_4(CO)_{13}]^-$ species. Similarly, the decomposition of $K[Fe_2Mn(CO)_{12}]$ in He produced no detectable intermediates, but under $H_2$ it led to the formation of these same two intermediate clusters, while $K[HFe_3(CO)_{11}]$ yielded $[HFe_4(CO)_{13}]^-$. First-order rate constants of decomposition were determined for each cluster, compared to literature $k_1$ values for nucleophilic substitution reactions in solution, and found to be similar to substitution rate constants for $Fe_3(CO)_{12}$ and $Mn_2(CO)_{10}$ but higher than those for $Fe(CO)_5$. The rate-determining step in either the substitution or the decomposition reaction appears to be the removal of the first CO ligand in $Fe_3(CO)_{12}$, but with $Mn_2(CO)_{10}$ it is Mn–Mn bond scission. The activation energies of decomposition were 18–21 kcal/mol for $Fe_3(CO)_{12}$ and 32–40 kcal/mol for $Mn_2(CO)_{10}$, while those for the decomposition products gave intermediate values. This study represents a portion of the first successful application of an IR spectroscopic technique to characterize carbon-supported metal catalysts. 

## INTRODUCTION

The hydrogenation of CO to form hydrocarbons is a well-known reaction and has received considerable attention in the past (*1, 2*); however, the achievement of high selectivity to higher value products, such as low-molecular-weight olefins, still remains as a challenge in catalysis. Numerous catalysts have been developed to try to overcome this limitation (*3–14*), and a relatively recent advance in this area was the development of bulk olefin-selective Fe–Mn catalysts (*15, 16*). Subsequent studies of Fe–Mn systems have included coprecipitated (*17–44*), alloy (*44*), oxide-supported (*45–54*), and carbon-supported (*55, 56*) Fe–Mn catalysts. Although exceptions exist, Fe–Mn systems routinely give high selectivities to olefins from syngas and therefore have commercial potential. The reasons for this enhancement are not clear although several postulates have been made regarding the state of the catalyst. Schulz and co-workers (*39, 40, 44*) have described it as small Fe particles supported in an oxide matrix, i.e., a structural promotion, while Abbot *et al.* view it as a combination of structural and electronic promotion (*49*). Others have proposed the existence of mixed Fe–Mn oxide phases under reaction conditions to explain the high selectivity (*31–35, 55, 56*). There is evidence that olefin formation seems to be related to the intimacy of contact between Fe and Mn prior to activation procedures, so that the selectivity is maximized when

[1] To whom correspondence should be addressed.



0021-9517/89 $3.00

the Fe–Mn interfacial area is maximized. This has been illustrated by using a bulk $Fe_2MnO_4$ spinel as the catalyst precursor and obtaining high olefin yields (*41*).

The few studies dealing with supported Fe–Mn systems derived from mixed-metal carbonyl clusters (MCCs) have concerned themselves with the kinetic behavior of these systems rather than their activation and chemical state (*50, 51, 55, 56*). A significant advantage of using MCCs as precursors is that the metals are in a zero-valent state, and the interaction between the Fe and Mn atoms and their CO ligands can be monitored using IR spectroscopy; however, no such studies have been reported for Fe–Mn clusters. Carbon can be treated at high temperatures to remove hydroxyl and carboxyl groups (*57, 58*), thereby eliminating the oxidation of these metal clusters that has been observed on oxide supports. Unfortunately, the opaque nature of carbon has not allowed the use of routine IR spectroscopic techniques to characterize these supported clusters as is done with oxide supports; however, the recent development of diffuse reflectance infrared Fourier transform spectroscopy (DRIFTS) and improvements in cells to enhance sensitivity and allow *in situ* pretreatments now provide the opportunity to study the decomposition of metal carbonyl clusters on carbon and the resulting metal/carbon catalysts (*59, 60*). Here we quantitatively describe the decarbonylation of carbon-supported $Mn_2(CO)_{10}$, $N(C_2H_5)_4$ $[Fe_2Mn(CO)_{12}]$, $K[Fe_2Mn(CO)_{12}]$, and $K[HFe_3(CO)_{11}]$ by obtaining rate constants and activation energies for the decomposition reactions and comparing them to values for $Fe_3(CO)_{12}$. The reduced Fe particles formed by this process are then characterized by CO adsorption and DRIFTS spectra of this CO on the Fe surface. Further characterization of these same catalysts by Mössbauer spectroscopy and STEM/EDS is described in the next paper in this series (*61*), while the kinetic and adsorption behavior, the CO heats of adsorption for these catalysts, and the chemical species associated with the genesis of these catalysts, as indicated from this multitechnique approach, are discussed in the third paper (*62*).

## EXPERIMENTAL

The amorphous carbon black used as a support in this study was CSX-203 from Cabot Corporation (now available as Black Pearls 2000). Sulfur and oxygen were removed by treatment in $H_2$ at 1223 K for 12 h (*63, 64*), and the carbon was stored in a glovebox. The $Fe_3(CO)_{12}$ and $Mn_2(CO)_{10}$ (Strem Chemical Co.) were used as received. $NEt_4[Fe_2Mn(CO)_{12}]$ (*65*), $K[Fe_2Mn(CO)_{12}]$ (*65*), and $K[HFe_3(CO)_{11}]$ (*66*) clusters were prepared using published methods. Before impregnation the carbon was heated to 673 K under dynamic vacuum ($10^{-4}$ kPa) for 8 h. The carbon was cooled in an ice water–salt bath and the MCCs were added by an incipient wetness impregnation technique using dry, degassed THF as solvent. The solution was introduced under nitrogen using standard Schlenk techniques (*67*), after which the remaining solvent was removed by evacuation to $10^{-4}$ kPa for 8 h at 300 K. Following the evacuation procedure, the catalyst was stored in a glovebox under $N_2$. Final metal loadings were determined by analysis after slow ashing of the carbon support. These values, both before and after HTR, were routinely close to the initial loadings.

The infrared spectra were collected on a Mattson Instruments Sirius 100 FTIR with $N_2$ purging using an extensively modified version of a Harrick Scientific HVC-DRP DRIFTS cell, which was coupled to a praying mantis DRA-2CS mirror assembly described elsewhere (*60, 68, 69*). The DRIFTS samples were prepared by mixing the carbon-supported clusters with precalcined, $H_2$-treated $CaF_2$ inside the glovebox using a $CaF_2$ : C dilution ratio of 200 : 1 and loading the DRIFTS cell inside the glovebox prior to connecting the cell to the FTIR without air exposure. A single batch of catalyst was used for DRIFTS experi-

ments on $Fe_3(CO)_{12}$/C, $K[HFe_3(CO)_{12}]$/C, $K[Fe_2Mn(CO)_{12}]$/C, and $Mn_2(CO)_{10}$/C, but two batches were used for the $NEt_4[Fe_2Mn(CO)_{12}]$/C studies—one for decarbonylation in He and another for decarbonylation in $H_2$.

Rates of decarbonylation were measured in $H_2$ and also in He at various constant temperatures after which the samples were heated to 473 K in the same gas for 2 h and cooled. Then CO was introduced and spectra of adsorbed CO were obtained at 195 and 300 K on these fully decarbonylated catalysts. Following these measurements the samples were subjected to a high-temperature reduction (HTR) by heating to 673 K in flowing $H_2$, reducing for 16 h, flushing in $H_2$ or He at 673 K for 30 min, cooling to 300 K, and scanning at both 300 and 195 K for adsorbed CO. The catalysts were also investigated after reduction conditions. The samples were cooled to 300 K and a background spectrum was collected; then they were exposed to 11 Torr CO in 749 Torr $H_2$, heated to 523 K for 2 h, cooled to 300 K, and a spectrum was collected to determine the presence of species containing $CH_x$ groups.

The fully decarbonylated catalyst in the absence of CO at each temperature utilized was used as the background material to collect background spectra. The FTIR parameters were set at a resolution of 4 $cm^{-1}$. The decarbonylation spectra were obtained by signal-averaging 100–1000 scans. The background spectra in all cases were obtained by averaging 10,000 scans. Data manipulation consisted of ratioing the sample and background spectra to obtain the transmittance spectra, calculating the absorbance files, and baseline-correcting the absorbance files which were then used to calculate baseline-corrected transmittance files from which the diffuse reflectance files (in Kubelka–Munk units) were calculated. The spectra presented are in Kubelka–Munk (KM) units, $KM = (1 - R_0)^2/(2R_0 = kc/s$, where $R_0$ is the baseline-corrected transmittance spectrum, $k$ is the molar extinction coefficient, $c$ is the concentration, and $s$ is a scattering coefficient (*70*). Absorbance spectra calculated from the same data to verify baseline correction were essentially identical. Additional details and the results of many additional studies to determine the range of proportionality between KM intensity and concentration have been reported elsewhere (*69*).

## RESULTS

The catalyst metal loadings are listed in Table 1. The total metal loadings varied between 7.8 and 10.2 wt%, while the Fe loading varied between 5.0 and 8.7 wt%. Only one $Fe_3(CO)_{12}$/C catalyst, denoted as $Fe_3(CO)_{12}$—A, was investigated by DRIFTS, and the decarbonylation of $Fe_3(CO)_{12}$ on carbon was found to proceed via the rapid formation of small zero-valent Fe particles and $Fe(CO)_5$, with the latter decomposing more slowly to metallic iron (*71*). This decarbonylation study is discussed in detail elsewhere (*71*).

The decarbonylation of carbon-supported $Mn_2(CO)_{10}$ was investigated in flowing He and $H_2$, and a typical set of spectra for decomposition at 369 K in flowing He is shown in Fig. 1. The bands in the initial spectrum at 2047, 2025, 2012(s), and 1983 (w) $cm^{-1}$ are in excellent agreement with values for the cluster in solution, which are listed in Table 2 (*72–105*). This cluster decomposed straightforwardly under He with no formation of stable subcarbonyl species. First-order rate constants of decarbonyl-

TABLE 1

Metal Loadings of Carbon-Supported Catalysts Prepared from Metal Carbonyl Clusters

| Catalyst precursor | Weight loading (%) | | | | μmol metal/g cat | | |
|---|---|---|---|---|---|---|---|
| | Fe | Mn | K | Total | Fe | Mn | K |
| $Fe_3(CO)_{12}$—A | 8.7 | — | — | 8.7 | 1551 | — | — |
| $Fe_3(CO)_{12}$—B | 6.5 | — | — | 6.5 | 1150 | — | — |
| $NEt_4[Fe_2Mn(CO)_{12}]$ | 5.0 | 2.8 | — | 7.8 | 885 | 513 | — |
| $Mn_2(CO)_{10}$ | — | 8.0 | — | 8.0 | — | 1448 | — |
| $K[Fe_3(CO)_{11}]$ | 7.2 | — | 2.7 | 9.9 | 1284 | — | 704 |
| $K[Fe_2Mn(CO)_{12}]$ | 5.3 | 3.0 | 1.9 | 10.2 | 954 | 544 | 485 |

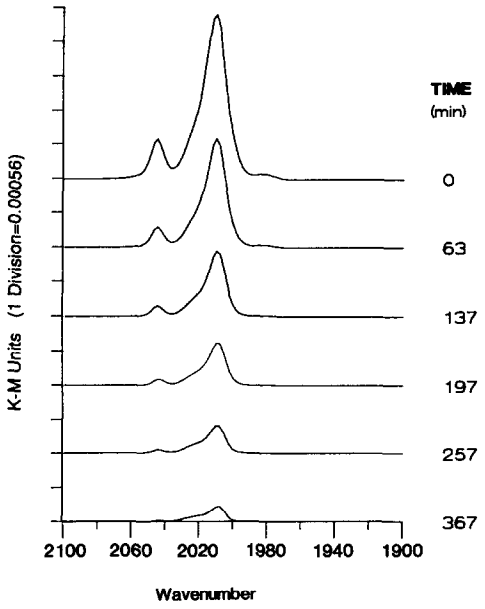


FIG. 1. Spectra of carbon-supported $Mn_2(CO)_{10}$ after various times in He at 369 K. The principal IR bands are at 2045 and 2012 $cm^{-1}$.

ation were determined from plots such as those in Fig. 2, which illustrate that this reaction was indeed first order, as expected. Decarbonylation in $H_2$ was investigated in similar fashion and typical spectra are shown in Fig. 3. Again, the initial spectrum indicated the presence of only $Mn_2(CO)_{10}$, which then decarbonylated in $H_2$ as it did in He. First-order kinetics again described the reaction well as shown in Fig. 4, and the rate constants determined from the slopes of these plots at different temperatures gave the Arrhenius plots in Fig. 5. The activation energies, $E_a$, and rate constants, $k$, for decarbonylation are summarized in Table 3. Activation energies of 32.0 and 32.7 kcal/mol were obtained for the 2012 and 2045 $cm^{-1}$ bands in $H_2$, respectively, and 36.9 kcal/mol was obtained for the 2012 $cm^{-1}$ band in He. The stability of the $Mn_2(CO)_{10}$ cluster is indicated by these higher $E_a$ values and much smaller rate constants compared to those for Fe carbonyl clusters, which are also given in Table 3.

The difference in behavior of a mixed-metal cluster is illustrated by the decomposition of $NEt_4[Fe_2Mn(CO)_{12}]$ in He, as shown in Fig. 6. The initial spectrum gave bands at 2002 and 1993 $cm^{-1}$, in good agreement with the principal bands for the clus-

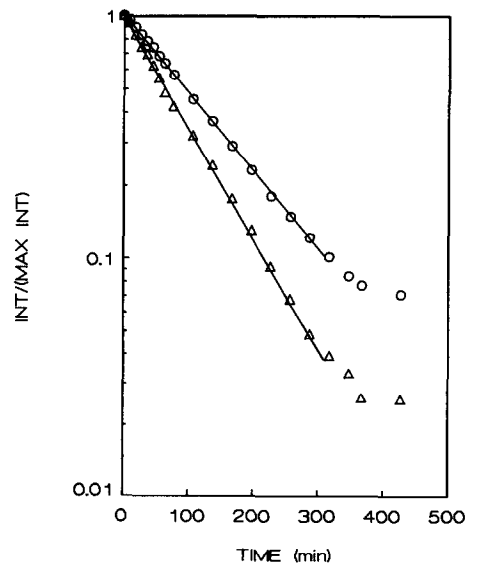


FIG. 2. Rate of decarbonylation of carbon-supported $Mn_2(CO)_{10}$ in He at 369 K: △, 2045 $cm^{-1}$ band; ○, 2012 $cm^{-1}$ band.

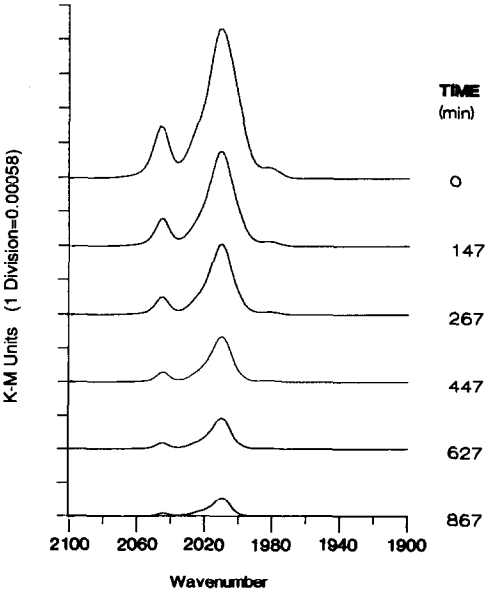


FIG. 3. Spectra of carbon-supported $Mn_2(CO)_{10}$ after various times in $H_2$ at 395 K. The principal IR bands are at 2045 and 2012 $cm^{-1}$.

TABLE 2

Reported IR Bands of Fe, Mn, and Fe–Mn Carbonyl Clusters in Solution

| Cluster | Wavenumber ($cm^{-1}$) | | | | Reference |
|---|---|---|---|---|---|
| $Fe(CO)_5$ | **2019–2033**[c] | **1995–2000** | | | *72–79* |
| $Fe(CO)_4L$[a] | 2040–2099 | 1970–2018 | **1933–1963** | | *73, 74, 79, 80* |
| $Fe(CO)_4L$[b] | 2099 | **2018** | **2000** | | *74* |
| $Fe(CO)_3L_2$ | **1877–1925** | | | | *74, 79, 80* |
| $[Fe(CO)_4]^{2-}$ | 2005 | 1962 | **1730–1786** | | *81–84* |
| $[HFe(CO)_4]^-$ | 2008 | 1910–1914 | **1840–1897** | | *81, 83, 85* |
| $Fe_2(CO)_9$ | **2064–2065** | **2015–2037** | 1828–1847 | | *86, 87* |
| $[Fe_2(CO)_8]^{2-}$ | **1916–1920** | **1852–1866** | | | *81, 85* |
| $[HFe_2(CO)_8]^-$ | 2068 | 2048 | 1980–1997 | **1923–1930** | *81, 85* |
| $Fe_3(CO)_{12}$ | 2097–2103 | **2043–2056** | **2013–2026** | | *73, 75, 88–93* |
| $Fe_3(CO)_{11}L$ | 2070–2092 | 2025–2035 | **2008–2011** | 1993–1998 | *80, 94* |
| $Fe_3(CO)_{10}L_2$ | 2062–2068 | **2013–2023** | **1995–2003** | 1957–1978 | *80, 94* |
| $Fe_3(CO)_9L_3$ | 2040–2049 | **1974–1986** | 1814–1829 | 1770–1788 | *80, 94* |
| $[Fe_2(CO)_{11}]^{2-}$ | 2000–2010 | **1931–1943** | 1900–1913 | 1880–1884 | *75, 81, 85, 95* |
| $[HFe_3(CO)_{11}]^-$ | 2075–2062 | **2000–2012** | **1970–1980** | 1942–1961 | *75, 81, 85, 92, 95–100* |
| $[Fe_4(CO)_{13}]^{2-}$ | 2067–2068 | 2021–2030 | 1990–2009 | **1938–1950** | *81, 85* |
| $[HFe_4(CO)_{13}]^-$ | **2020–2031** | **1980–1984** | 1961 | **1936–1942** | *81, 85* |
| $Mn_2(CO)_{10}$ | 2043–2045 | **2012–2014** | 1983 | | *74, 101, 103* |
| $Mn_2(CO)_9L$ | **2037** | **2013** | 1979 | | *74* |
| $Mn_2(CO)_8L_2$ | 2028 | **2011** | | | *74* |
| $[Mn(CO)_5]^-$ | **1896–1898** | **1862–1863** | | | *104* |
| $[Fe_2Mn(CO)_{12}]^-$ | 2063–2064 | **1999** | **1989–1990** | 1972–1975 | *96*, this work |
| $[FeMn(CO_9)]^-$ | 2066–2070 | 1995–2024 | **1968–1973** | 1937–1943 | *65* |
| $Mn_2Fe(CO)_{14}$ | **2067** | **2019** | 1987 | | *105* |

[a] Axial L.

[b] Equatorial L.

[c] Wavenumbers in boldface represent major bands.

ter in solution (see Table 2). The decomposition of this cluster in He at 330 K proceeded with a retention of bands in the region 1960–2020 $cm^{-1}$, and it was very well described by first-order kinetics, as shown in Fig. 7, with the 2002 and 1993 $cm^{-1}$ bands giving similar slopes. Decarbonylation studies in He of the first $NEt_4[Fe_2Mn(CO)_{12}]/C + CaF_2$ mixture were completed, but a second mixture was required for decarbonylation in $H_2$ because no bands were detected in the first sample after 2 weeks of storage in the glovebox.

The decomposition in $H_2$ of the cluster in this mixture was studied and a typical set of spectra is given in Fig. 8, which shows initial bands at 2045, 2008, and 1993 $cm^{-1}$. As decarbonylation proceeded, the band intensities at 2045, 2010–2020, 1970–1980, and 1930–1940 $cm^{-1}$ increased. As discussed later, the bands at 2045 and 2025 $cm^{-1}$ are due to $Mn_2(CO)_{10}$, the band near 2012 $cm^{-1}$ contains contributions from both $Mn_2(CO)_{10}$ and $NEt_4[Fe_2Mn(CO)_{12}]$, and the weak bands near 1980 and 1940 $cm^{-1}$ are attributed to a decomposition product, $[HFe_4(CO)_{13}]^-$. The shoulder at 1993 $cm^{-1}$ is due to the $[Fe_2Mn(CO)_{12}]^-$ anion.

The intensities of these three bands versus time are plotted in Fig. 9. The 2045 $cm^{-1}$ band grew with time, indicating that $Mn_2(CO)_{10}$, was a product of decomposition

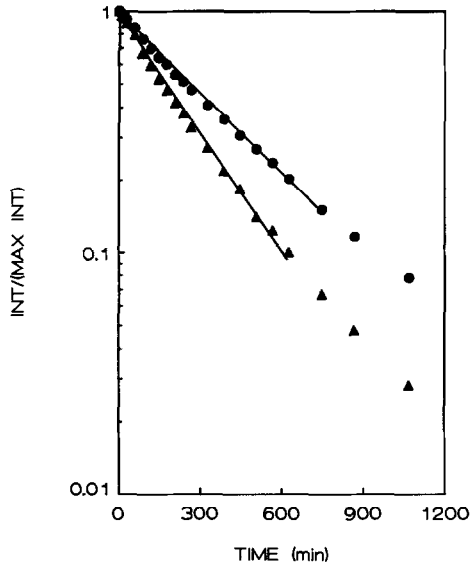


FIG. 4. Rate of decarbonylation of carbon-supported $Mn_2(CO)_{10}$ in $H_2$ at 359 K: ▲, 2045 $cm^{-1}$ band; ●, 2012 $cm^{-1}$ band.

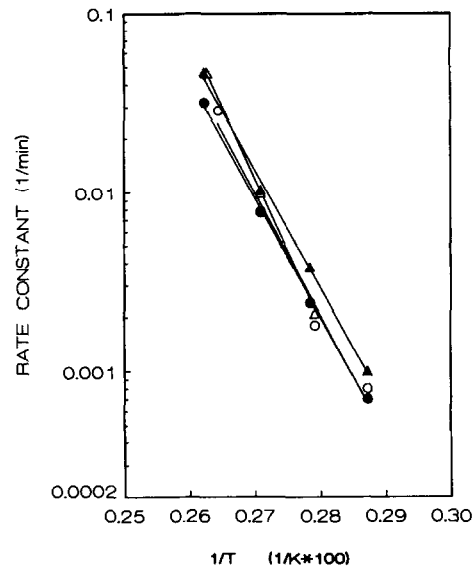


FIG. 5. Arrhenius plots for the decarbonylation of carbon-supported $Mn_2(CO)_{10}$. △, 2045 $cm^{-1}$ band in He; ○, 2012 $cm^{-1}$ band in He; ▲, 2045 $cm^{-1}$ band in $H_2$; ●, 2012 $cm^{-1}$ band in $H_2$.

of the $[Fe_2Mn(CO)_{12}]^-$ anion. Also, the plot of the 1993 $cm^{-1}$ intensity indicates that first-order kinetics satisfactorily describes the initial decomposition process, but after long reaction times the contribution of the 2012 $cm^{-1}$ band of $Mn_2(CO)_{10}$ to the intensity at 1993 $cm^{-1}$ became significant and caused a deviation from the initial slope.

TABLE 3

Activation Energies and Rate Constants for Decomposition of Carbon-Supported K–Fe–Mn MCCs in $H_2$ and He

| Initial cluster | IR band ($cm^{-1}$) | $k_1$ at 350 K[a] ($min^{-1}$) | | Activation energy (kcal/mol) | |
|---|---|---|---|---|---|
| | | He | $H_2$ | He | $H_2$ |
| $Fe_3(CO)_{12}$[b] | 2045 | 0.52 | 2.3 | 17.9 | 21.3 |
| $Fe(CO)_5$[b] | 2000 | 0.15 | 0.37 | 15.3 | 15.7 |
| $NEt_4[Fe_2Mn(CO)_{12}]$ | 2045 | —[c] | —[d] | — | — |
| | 2002 | 0.06 | — | 15.9 | — |
| | 1993 | 0.06 | 0.20 | 15.9 | 18.2 |
| $Mn_2(CO)_{10}$ | 2045 | 0.0006 | 0.0014 | 40.5 | 32.7 |
| | 2012 | 0.0006 | 0.0009 | 36.9 | 32.0 |
| $K[HFe_3(CO)_{11}]$ | 2010 | 0.18 | 0.16 | 17.1 | 18.3 |
| $K[Fe_2Mn(CO)_{12}]$ | 2045 | 0.0030 | 0.0030 | 24.3 | 24.3 |
| | 1993 | 0.15 | 0.15 | —[e] | 18.8 |

[a] Extrapolated from Arrhenius plot.
[b] From Ref. (*71*).
[c] The decomposition in He showed no 2045 $cm^{-1}$ band and both bands are due to the original cluster.
[d] Very weak; not quantitatively followed.
[e] Not determined; only two $k_1$ values obtainable.

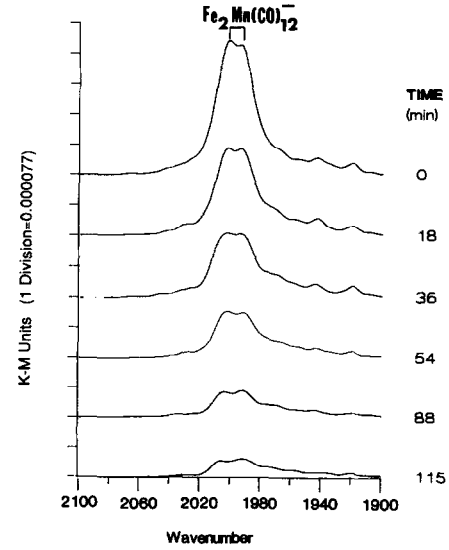


FIG. 6. Spectra of carbon-supported $NEt_4[Fe_2Mn(CO)_{12}]$ after various times in He at 330 K. The principal IR bands are at 2002 and 1993 $cm^{-1}$.

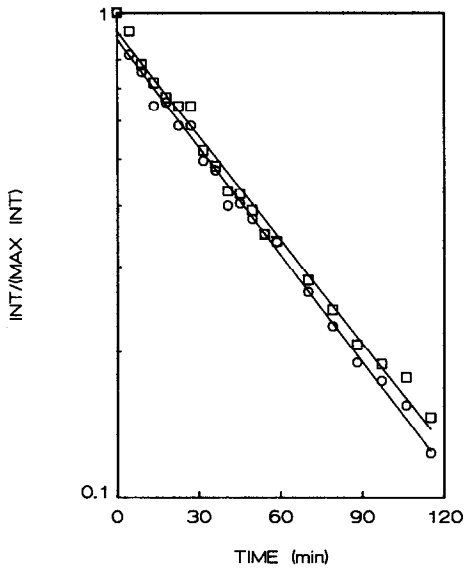


FIG. 7. Rate of decarbonylation of carbon-supported $NEt_4[Fe_2Mn(CO)_{12}]$ in He at 330 K. ○, 2002 $cm^{-1}$ band; □, 1993 $cm^{-1}$ band.

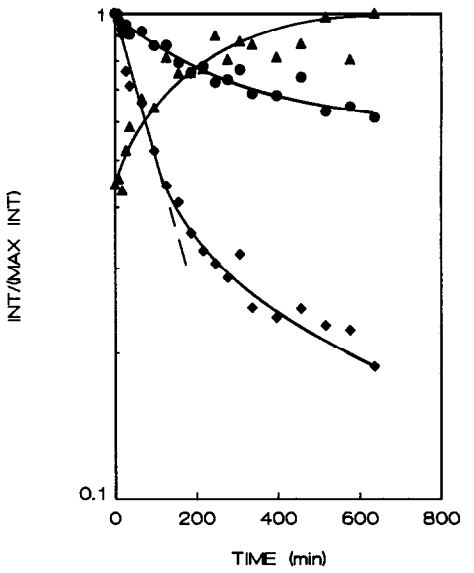


FIG. 9. Changes in band intensities of carbon-supported in $NEt_4[Fe_2Mn(CO)_{12}]$ in $H_2$ at 314 K. ▲, 2045 $cm^{-1}$ band; ●, 2010 $cm^{-1}$ band; ◆, 1993 $cm^{-1}$ band.

The 2012 $cm^{-1}$ band intensity contained contributions from both species and followed intermediate behavior, as expected.

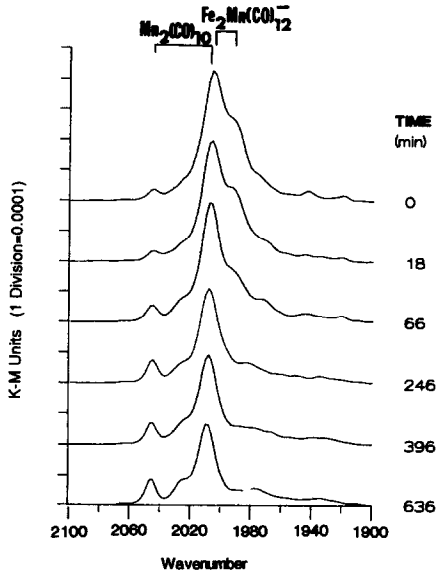


FIG. 8. Spectra of carbon-supported $NEt_4[Fe_2Mn(CO)_{12}]$ after various times in $H_2$ at 314 K. The initial principal IR bands were at 2045, 2010, and 1993 $cm^{-1}$.

This pattern was independent of the decomposition temperature (*69*).

During the initial time periods, the 1993 $cm^{-1}$ band intensity was representative of the anionic precursor concentration, and the initial slopes at various temperatures were used to determine the rate constants of decomposition which are given in the Arrhenius plots in Fig. 10. The reaction in He readily yielded an activation energy of 15.9 kcal/mol, but it was more complex in $H_2$ and only the 1993 $cm^{-1}$ band could be used for quantitative rate measurements, from which a similar activation energy of 18.2 kcal/mol was determined. These activation energies are close to those obtained for $Fe(CO)_5$ but much lower than those for $Mn_2(CO)_{10}$.

The effect of potassium on the decarbonylation process was studied by investigating $K[HFe_3(CO)_{11}]$ and $K[Fe_2Mn(CO)_{12}]$ clusters dispersed on this carbon. A comparison of the behavior of $K[HFe_3(CO)_{11}]$ to that of $Fe_3(CO)_{12}$ must be done with caution, as the latter is a neutral cluster whereas the former contains an anionic

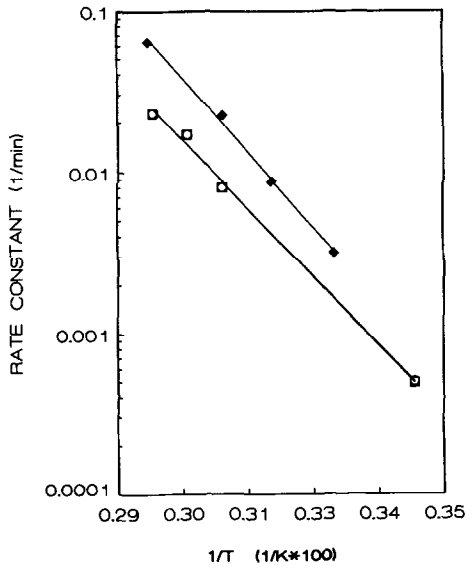


FIG. 10. Arrhenius plots for the decarbonylation of carbon-supported $NEt_4[Fe_2Mn(CO)_{12}]$. ○, 2002 $cm^{-1}$ band in He; □, 1993 $cm^{-1}$ band in He; ♦, 1993 $cm^{-1}$ band in $H_2$.

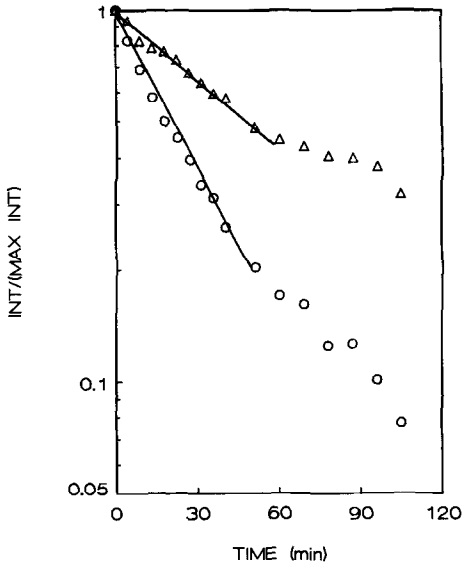


FIG. 12. Rates of decarbonylation of carbon-supported $K[HFe_3(CO)_{11}]$ in He at 325 K. ○, 2010 $cm^{-1}$ band; △, 1977 $cm^{-1}$ band.

$[HFe_3(CO)_{11}]^-$ species containing hydrogen. An example of the decarbonylation of $K[HFe_3(CO)_{11}]$ in flowing He at 323 K is represented in Fig. 11. The initial cluster had bands at 2010 and 1977 $cm^{-1}$, in good agreement with the major bands listed in Table 2 for $[HFe_3(CO)_{11}]^-$ in solution. The initial decarbonylation in He again conformed to first-order kinetics, as shown in Fig. 12, with the 2010 $cm^{-1}$ band being preferable due to its greater intensity. Decarbonylation in $H_2$ at 334 K, shown in Fig. 13 as a typical example, proceeded with a retention of intensity in the region 2020–1930 $cm^{-1}$, indicative of small amounts of partially decarbonylated products. The first-order kinetic plots of these relative band intensities are shown in Fig. 14, and the Arrhenius plots obtained from their initial slopes are shown in Fig. 15. The decarbonylation rates were similar under either He or $H_2$, particularly for the principal band, and the $E_a$ values of 17.1 kcal/mol in He and 18.3 kcal/mol in $H_2$ for the disappearance of the 2010 $cm^{-1}$ band were also similar. No $Fe(CO)_5$ was detected during the decarbonylation process and, as expected, no bands grew at 2045 and 2010 $cm^{-1}$ because of the absence of Mn in the cluster.

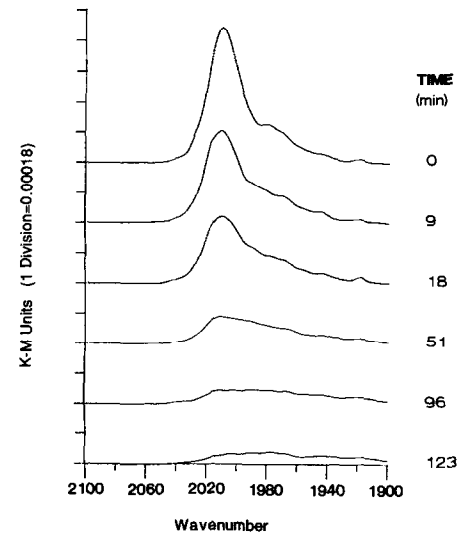


FIG. 11. Spectra of carbon-supported $K[HFe_3(CO)_{11}]$ after various times in He at 325 K. The principal IR bands are at 2010 and 1977 $cm^{-1}$.

The influence of K on the decomposition

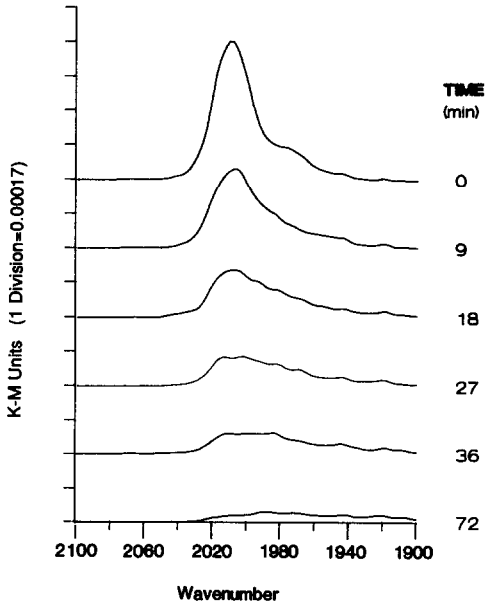


FIG. 13. Spectra of carbon-supported $K[HFe_3(CO)_{11}]$ after various times in $H_2$ at 334 K. The principal IR bands are at 2010 and 1977 $cm^{-1}$.

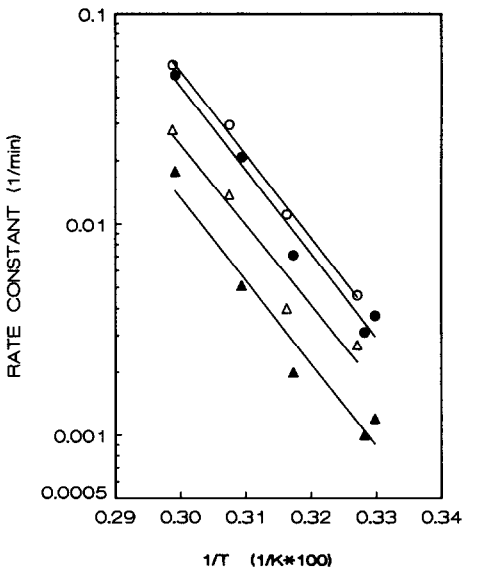


FIG. 15. Arrhenius plots for the decarbonylation of carbon-supported $K[HFe_3(CO)_{11}]$. ○, 2010 $cm^{-1}$ band in He; △, 1977 $cm^{-1}$ band in He; ●, 2010 $cm^{-1}$ band in $H_2$; ▲, 1977 $cm^{-1}$ band in $H_2$.

process of a mixed-metal cluster is illustrated by a comparison of $K[Fe_2Mn(CO)_{12}]$ and $NEt_4[Fe_2Mn(CO)_{12}]$, as they contain the same anion. The decarbonylation and the behavior of $K[Fe_2Mn(CO)_{12}]$ in He at 328 K are typified in Fig. 16. The initial spectrum had well-resolved bands at 2045 and 2010 $cm^{-1}$ and a shoulder at 1993 $cm^{-1}$.

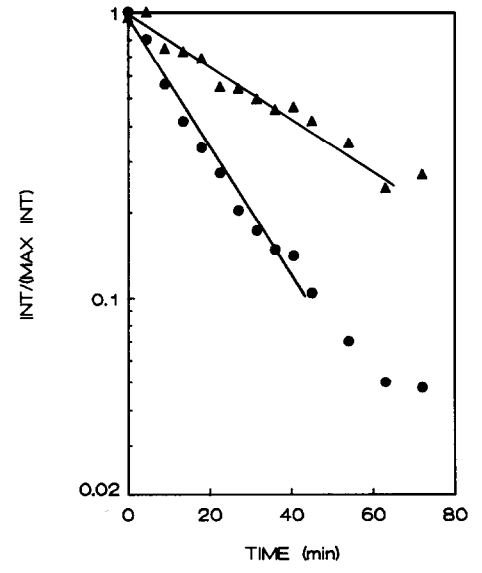


FIG. 14. Rates of decarbonylation of carbon-supported $K[HFe_3(CO)_{11}]$ in $H_2$ at 334 K. ●, 2010 $cm^{-1}$ band; ▲, 1977 $cm^{-1}$ band.

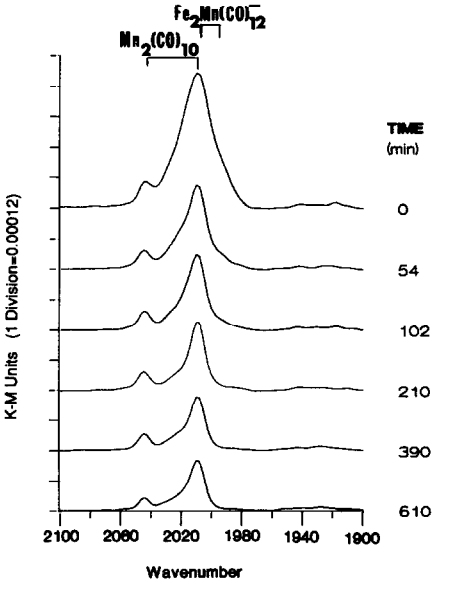


FIG. 16. Spectra of carbon-supported $K[Fe_2Mn(CO)_{12}]$ after various times in He at 328 K. The principal IR bands are at 2045, 2010, and 1993 $cm^{-1}$.

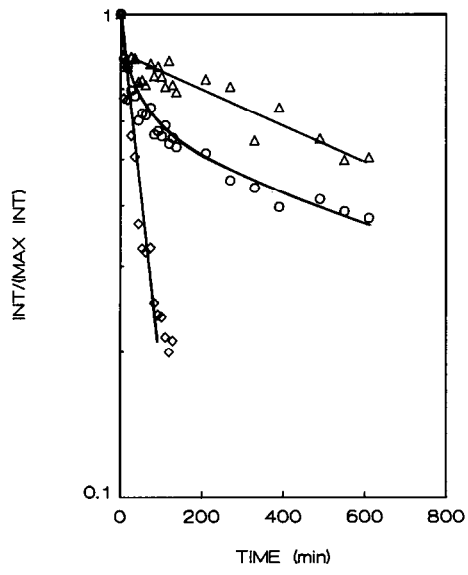


FIG. 17. Rates of decarbonylation of carbon-supported $K[Fe_2Mn(CO)_{12}]$ in He at 328 K: △, 2045 $cm^{-1}$ band; ○, 2010 $cm^{-1}$ band; ◇, 1993 $cm^{-1}$ band.

The reaction proceeded and gave residual bands at 2045 and 2010 $cm^{-1}$ after disappearance of the intensity at 1993 $cm^{-1}$. The decomposition of this cluster produced the same band intensity behavior as described for the $NEt_4[Fe_2Mn(CO)_{12}]$ cluster, as shown in Fig. 17. Spectra of the decarbonylation of $K[Fe_2Mn(CO)_{12}]$ in $H_2$ at 327 K are given in Fig. 18 and the relative intensities in Fig. 19 indicate an initial decrease, then an increase in intensity of the band at 2045 $cm^{-1}$ and in the 2010 and 1985 $cm^{-1}$ regions while the band at 1993 $cm^{-1}$ decreased rapidly. This general decarbonylation behavior was again independent of the temperature (*69*), and it indicates that the decomposition reaction is kinetically limited and not constrained by equilibrium considerations. The rate constants used to obtain activation energies of decarbonylation are given in Fig. 20. The decomposition of $K[Fe_2Mn(CO)_{12}]$ on carbon clearly yielded two species that decarbonylated at two distinctly different rates, namely a species with a band at 1993 $cm^{-1}$, and a species with bands at 2045 and 2010 $cm^{-1}$. The former, associated with the initial cluster, had an $E_a$ of 19 kcal/mol under either He or $H_2$, while the latter bands, associated with $Mn_2(CO)_{10}$, gave a value near 24 kcal/mol.

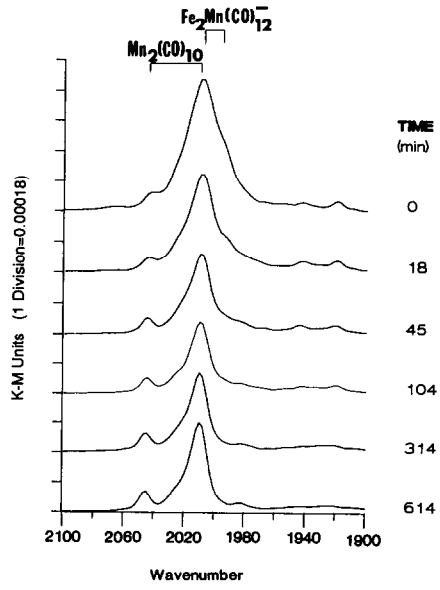


FIG. 18. Spectra of carbon-supported $K[Fe_2Mn(CO)_{12}]$ after various times in $H_2$ at 327 K. The principal IR bands are at 2045, 2010, and 1993 $cm^{-1}$.

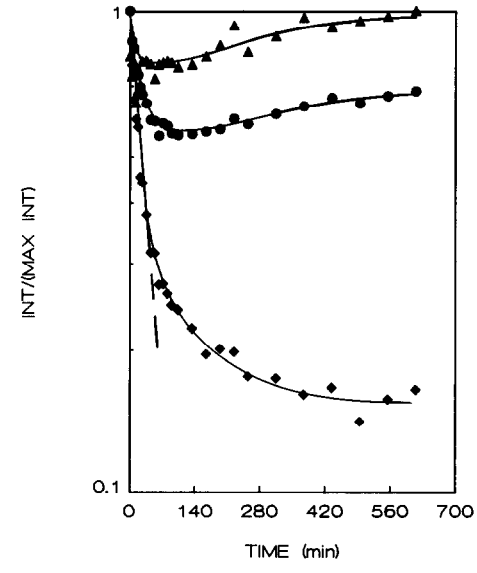


FIG. 19. Changes in band intensity during decarbonylation of carbon-supported $K[Fe_2Mn(CO)_{12}]$ in $H_2$ at 327 K: ▲, 2045 $cm^{-1}$ band; ●, 2010 $cm^{-1}$ band; ◆, 1993 $cm^{-1}$ band.

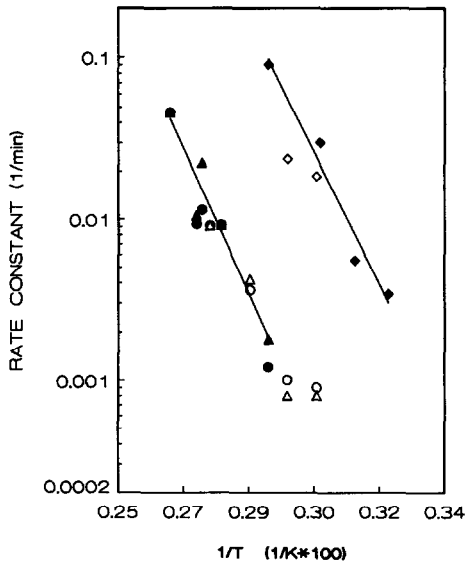


FIG. 20. Arrhenius plots for the decarbonylation of carbon-supported $K[Fe_2Mn(CO)_{12}]$. △, Band at 2045 $cm^{-1}$ in He (final slopes); ○, band at 2010 $cm^{-1}$ in He (final); ◇, band at 1993 $cm^{-1}$ in He (initial slopes); ▲, band at 2045 $cm^{-1}$ in $H_2$ (final); ●, band at 2010 $cm^{-1}$ in $H_2$ (final); ◆, band at 1993 $cm^{-1}$ in $H_2$ (initial).

Two further observations should be made at this point. The first is that a significant growth of the 2045 $cm^{-1}$ peak was not observed when either $NEt_4[Fe_2Mn(CO)_{12}]$ or $K[Fe_2Mn(CO)_{12}]$ was decomposed in He, but both MCCs showed a growth of this peak when decomposed in $H_2$; therefore, $H_2$ appears to facilitate a pathway that gives $Mn_2(CO)_{10}$ as an intermediate. A second observation is that the $NEt_4[Fe_2Mn(CO)_{12}]$ species remained essentially intact during impregnation and later in flowing He, but some decomposition of the $K[Fe_2Mn(CO)_{12}]$ cluster occurred during the impregnation step to form $Mn_2(CO)_{10}$, thus giving the 2045 $cm^{-1}$ band. The presence of K apparently enhances cluster decomposition to form the intermediate $Mn_2(CO)_{10}$ species with characteristic bands at 2045 $cm^{-1}$ and near 2010 $cm^{-1}$.

The adsorption of CO was investigated on all the catalysts after decomposition then reduction at 673 K in $H_2$, and the spectra for the four Fe-containing catalysts are shown in Fig. 21. All the spectra were collected under CO (11 Torr) in flowing He or $H_2$ (749 Torr). Gas-phase CO and CO weakly adsorbed on the carbon (2042 $cm^{-1}$) were subtracted out using spectra obtained separately on a $CaF_2$-diluted, carbon-only sample. As discussed elsewhere (*71*), adsorption of CO on $Fe_3(CO)_{12}$/C at 300 K after HTR in either $H_2$ or He caused the reformation of $Fe(CO)_5$, whereas no species were detected after a low-temperature reduction (LTR) at 473 K. The $Mn_2(CO)_{10}$ catalyst did not exhibit any adsorbed CO species in $CO/H_2$ or CO/He mixtures at either 195 or 300 K after either pretreatment, in agreement with CO adsorption measurements on this catalyst which showed no uptake (*62*). The addition of Mn to the cluster decreases $Fe(CO)_5$ formation, and the presence of K further decreases it, with only very low concentrations present in the $KFe_3$/C catalyst. Purging in pure He or $H_2$ removed these pentacarbonyl bands.

Figure 22 shows the spectra obtained at 300 K after the samples were exposed to

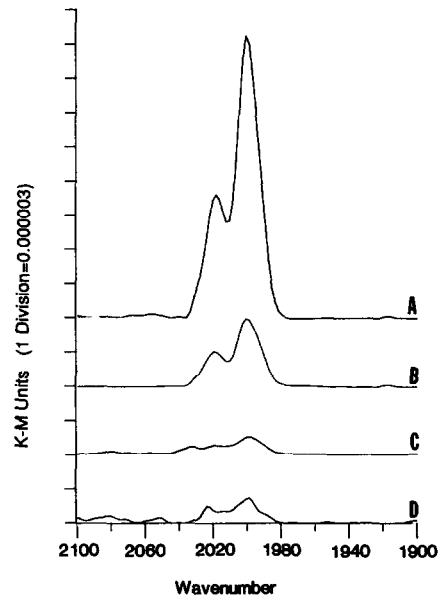


FIG. 21. Spectra of CO adsorbed at 300 K on Fe–Mn/C catalysts in 11 Torr CO, which indicate $Fe(CO)_5$ with bands at 2020 and 2000 $cm^{-1}$. (A) Fe/C, (B) $Fe_2Mn$/C, (C) $KFe_3$/C, (D) $KFe_2Mn$/C.

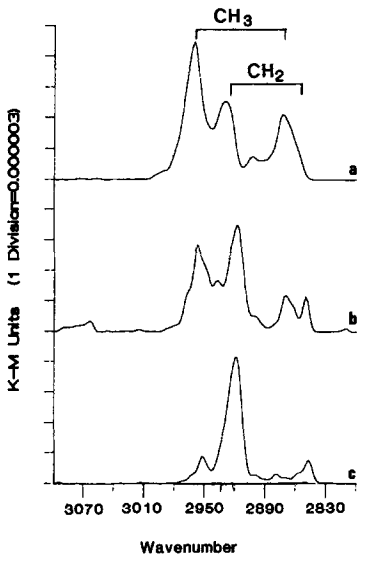


FIG. 22. IR spectra at 300 K following reaction conditions and cooling in a $CO/H_2$ mixture: (a) Fe/C, (b) $Fe_2Mn/C$, (c) $KFe_3/C$.

reaction conditions and cooled in 11 Torr CO and 749 Torr $H_2$. Spectrum A was obtained on Fe/C after HTR and exposure to CO and $H_2$ at 523 K for 2 h. Bands were observed at 2961, 2933, and 2874 $cm^{-1}$. Spectrum B is for $Fe_2Mn/C$ at 300 K following HTR and exposure to CO and $H_2$ for 2 h at 473, 523, and 573 K. The only bands observed were at 2961, 2932, 2874, and 2850 $cm^{-1}$. Spectrum C was obtained on $KFe_3/C$ following reaction at the above gas composition at 523 K for 2 h, and principal bands were again at 2961, 2932, and 2850 $cm^{-1}$. None of these catalysts exhibited bands between 1800 and 2100 $cm^{-1}$, but the bands observed agree well with reported values of 2875 and 2960 $cm^{-1}$ for $CH_3$ groups and 2850 and 2925 $cm^{-1}$ for $CH_2$ groups (*106–108*). No peaks were detectable under reaction conditions.

## DISCUSSION

Although many studies of Fe and Mn carbonyl clusters in solution and on solid surfaces have appeared in the literature, no investigation of the thermal decomposition of any cluster has been reported. Also, no studies of the behavior of Fe–Mn and K–Fe–Mn clusters on carbon exist although cluster-derived Fe–Mn/C and K–Fe–Mn/C catalysts have been prepared and characterized (*55, 56*). As mentioned in the Introduction, the highly opaque nature of carbon has precluded the use of IR spectroscopy for characterization in the routine manner employed in studies of oxide-supported clusters. However, the advent of DRIFTS along with improved cells to enhance sensitivity and provide *in situ* pretreatment capabilities (*59, 60, 68, 71*) has finally allowed the examination of C-supported clusters by an IR technique. In addition, our capability to prepare extremely clean carbon surfaces, free from oxygen-containing groups, provided the opportunity to quantitatively follow the decomposition process of these clusters in the absence of any interaction with surface oxygen. This provides an opportunity to compare this preparative approach with others utilizing zero-valent metal atoms initially to produce supported Fe–Mn and Co–Mn catalysts, such as the solvated metal atom dispersion technique of Klabunde and co-workers, but using oxide supports (*109, 110*). Finally, the state of the Fe–Mn particles that remain after complete decomposition was probed by looking at the IR spectra of CO chemisorbed on their surfaces, obtaining chemisorption capacities, measuring the CO heat of adsorption on these crystallites, and determining their catalytic behavior in the CO hydrogenation reaction (*61, 62*). The DRIFTS results are discussed in this paper.

The thermal decarbonylation behavior of carbon-supported $Fe_3(CO)_{12}$ and $Fe(CO)_5$ has recently been studied in detail in our laboratory (*71*). Of the other four carbonyl clusters compared here, $Mn_2(CO)_{10}$ is the only one whose decarbonylation or nucleophilic substitution reactivity in solution has been examined. Other than our investigation of Os, Ru, and Fe dodecacarbonyl clusters (*68, 71*), the thermal decomposition behavior of supported metal carbonyl clusters (MCCs) has not been reported.

The decomposition of $Mn_2(CO)_{10}$ in solution has received some attention although the kinetics of this reaction have not been determined (*103, 111–117*). This MCC undergoes homolytic Mn–Mn bond fission prior to nucleophilic substitution which results in a mechanism different from that associated with the three dodecacarbonyls mentioned previously, which have as the rate-determining step the initial rupture of a M–CO bond prior to substitution of a ligand. This difference in chemistry gives a substantially higher activation energy of 36.9 kcal/mol for substitution of $PPh_3$ into $Mn_2(CO)_{10}$ (*103*), compared to 22–29 kcal/mol for $PPh_3$ substitution into $Fe_3(CO)_{12}$ (*71*). The oxidation of $Mn_2(CO)_{10}$ to Mn oxide and CO also gives a similar $E_a$ of 37.0 (*103*). The activation energies for carbon-supported $Fe_3(CO)_{12}$ were lower than that for substitution reactions in solution, while the values found here for carbon-supported $Mn_2(CO)_{10}$, 32–37 kcal/mol, are in good agreement with the values reported for nucleophilic substitution in solution. The substitution rate of $PPh_3$ into $Mn_2(CO)_{10}$ was 0.00006 $min^{-1}$ at 350 K, which is 10-fold lower than the values in this study but it is consistent in that both are much lower than the comparable values for $Fe_3(CO)_{12}$ (*71*). This is not surprising because Mn oxide is again the final product due to the high affinity of Mn for oxygen, whereas the lower $E_a$ values for $Fe_3(CO)_{12}$ decomposition on carbon were explained by the formation of metallic iron particles, which does not occur for substitution reactions in solution. This assumption of MnO formation is strongly supported by the recent EXAFS study of $Co–Mn/SiO_2$ catalysts by Klabunde and Imizu (*110*). The observance of this difference illustrates that DRIFTS is capable of probing the surface chemistry of MCCs on carbon even at the low intensities obtained.

The decarbonylation behavior of $NEt_4[Fe_2Mn(CO)_{12}]$ demonstrated in Figs. 6–10 represents the first quantitative study of the thermal decomposition of a mixed-metal cluster. The initial spectrum in He exhibited band maxima at 2002 and 1993 $cm^{-1}$, values about 3 $cm^{-1}$ higher than those for the cluster in solution (Table 2). The cluster decomposed in He without significant formation of $Mn_2(CO)_{10}$ as no 2045 $cm^{-1}$ band was observed. The decarbonylation in $H_2$, however, was more complex as some $Mn_2(CO)_{10}$ was present in the initial spectrum, which displayed bands at 2045, 2008, and 1993 $cm^{-1}$, indicating that some decomposition of the initial MCC had occurred during sample preparation. The shoulder at 1993 $cm^{-1}$ is expected for the $[Fe_2Mn(CO)_{12}]^-$ anion but the band at 2008 $cm^{-1}$ is the superposition of two peaks, namely the 2012 $cm^{-1}$ peak of $Mn_2(CO)_{10}$ and the 2002 $cm^{-1}$ peak of $NEt_4[Fe_2Mn(CO)_{12}]$. With these assignments the decarbonylation process shown in Fig. 9 represents the rapid decomposition of the original cluster and the formation of $Mn_2(CO)_{10}$ to increase the intensity at 2045 and 2010 $cm^{-1}$. The increase of this cluster concentration, which is very sensitive to oxidation, demonstrates one advantage of using these oxygen-free carbons, as zero-valent Mn atoms form Mn oxide in $Co–Mn/SiO_2$ catalysts (*110*).

The rate constants of decarbonylation of $NEt_4(Fe_2Mn(CO)_{12}]$ under $H_2$ were determined by evaluating the initial slopes of the changes in the 1993 $cm^{-1}$ intensity to minimize the complication of overlapping peaks. Figure 9 indicates that this is a valid approach for the first 150 min of reaction; then the contribution of the overlapping 2012 $cm^{-1}$ band of $Mn_2(CO)_{10}$ becomes significant. Furthermore, Fig. 8 indicates the formation of species giving bands near 2020–2030, 1970–1980, and 1930–1940 $cm^{-1}$ during decarbonylation in $H_2$. From the summary in Table 2 the single species most capable of providing these bands is $[HFe_4(CO)_{13}]^-$, although $[HFe_3(CO)_{11}]^-$ is a possibility. However, a concomitant Mössbauer effect spectroscopic (MES) investigation of this same catalyst obtained peaks associated with either $[HFe_4(CO)_{13}]^-$ or $[HFe_2(CO)_8]^-$ (*61*). Only the $[HFe_4(CO)_{13}]^-$ species provides results consistent with

both studies. Also, the absence of these bands under He supports the assignment to a H-containing cluster. Consequently, the initial decomposition products in $H_2$ appear to be $Mn_2(CO)_{10}$, the hydrido-tetrairon cluster $[HFe_4(CO)_{13}]^-$, and zero-valent Fe particles (*61*).

The activation energies of decomposition of the $NEt_4[Fe_2Mn(CO)_{12}]$ cluster are 15.9 kcal/mol in He and 18.2 kcal/mol in $H_2$, similar to values for $Fe_3(CO)_{12}$ and $Fe(CO)_5$, while the rate constants are 0.06 $min^{-1}$ in He and 0.2 $min^{-1}$ in $H_2$, which are about 10 times lower than comparable values for $Fe_3(CO)_{12}$/C, similar to those for $Fe(CO)_5$, and 100 times higher than those for $Mn_2(CO)_{10}$. Mn therefore seems to stabilize the $[Fe_2Mn(CO)_{12}]^-$ anion to a small extent compared to $Fe_3(CO)_{12}$.

Some idea of the influence of potassium on the decarbonylation behavior of the trinuclear Fe cluster is obtained from the study of the $K[HFe_3(CO)_{11}]$ cluster; however, the anionic, H-containing nature of this cluster complicates a direct comparison to $Fe_3(CO)_{12}$. The decarbonylation behavior in He or $H_2$ was straightforward, initially followed first-order kinetics, and ended with broad bands existing in the region 1900–2020 $cm^{-1}$, implying the presence of $[HFe_4(CO)_{13}]^-$. Although the DRIFTS work is not conclusive in this regard, MES results showed that this anion is the only one capable of producing both the DRIFTS and the MES spectra (*61*). The transformation of $[HFe_3(CO)_{11}]^-$ into $Fe(CO)_5$ was not observed as with $Fe_3(CO)_{12}$, which is consistent with the results of Hanson *et al.*, who found that $Fe_3(CO)_{12}$ on $Al_2O_3$ transformed quantitatively to $[HFe_3(CO)_{11}]^-$ via $Fe(CO)_5$ as an intermediate (*118*). Carbon supports appear to facilitate the decomposition of $Fe_3(CO)_{12}$ into $Fe(CO)_5$, but not the further transformation to $[HFe_3(CO)_{11}]^-$ because this reaction requires the presence of hydroxyl groups (*118*), which are absent on this carbon.

The activation energies for decarbonylation of $K[HFe_3(CO)_{11}]$, 17.1 kcal/mol in He and 18.3 kcal/mol in $H_2$, are very similar to those reported for $Fe_3(CO)_{12}$ and may indicate that the mechanism for this three-Fe-atom cluster is similar to that for $Fe_3(CO)_{12}$ and the $[Fe_2Mn(CO)_{12}]^-$ anion. The rate constant for decomposition in He was about a factor of 3 lower than that for $Fe_3(CO)_{12}$ and a factor of 3 higher than that for $NEt_4[Fe_2Mn(CO)_{12}]$. However, under $H_2$ the rate constant was over an order of magnitude lower and near that for $NEt_4[Fe_2Mn(CO)_{12}]$, which may be a consequence of the formation of the tetranuclear cluster.

Addition of both K and Mn to the cluster gives the decarbonylation behavior in He and $H_2$ shown in Figs. 16 and 18, where bands at 2045, 2020, 2010, and 1993 $cm^{-1}$ indicate the initial presence of both $Mn_2(CO)_{10}$ and the original cluster. In both cases rapid decomposition of the original cluster occurs and rate constants are the same. Under $H_2$, however, weak bands exist to indicate the presence of $[HFe_4(CO)_{13}]^-$ species. Furthermore, decarbonylation in $H_2$ leads to an initial increase in the intensity of the 2045 $cm^{-1}$ peak, contrary to decarbonylation in He. In fact, the apparent rate constants in He may well be overestimated because some of the intensity decrease is probably due to the overlapping 2010 $cm^{-1}$ band. Therefore, $H_2$ appears to facilitate formation of $Mn_2(CO)_{10}$ during decarbonylation.

The results in Fig. 20 indicate that two different species are present, with different activation energies and rate constants. The Arrhenius plots show that the activation energy associated with the disappearance of $K[Fe_2Mn(CO)_{12}]$ in $H_2$ (18.8 kcal/mol) agrees well with that of 18.2 kcal/mol for the decomposition of the same anion when in the $NEt_4[Fe_2Mn(CO)_{12}]$ cluster. The rate constants for each cluster in either He or $H_2$ compare favorably; however, the presence of only two rate measurements under He precludes an accurate $E_a$ determination. Regardless, the $K[Fe_2Mn(CO)_{12}]$ and $NEt_4[Fe_2Mn(CO)_{12}]$ clusters exhibit very similar

decomposition kinetics. This is consistent with the supposition that the rate-determining step is the rupture of the initial Fe–CO ligand, which should be similar because the anionic cluster is the same.

The decarbonylation of $Mn_2(CO)_{10}$ in the presence of Fe, as indicated by the bands at 2045 and 2010 $cm^{-1}$ with the $K[Fe_2Mn(CO)_{12}]$ precursor, gave a lower activation energy of 24.3 kcal/mol in He or $H_2$ compared to that of 32–37 kcal/mol obtained for the samples with only $Mn_2(CO)_{10}$. Also, the rate constants of 0.003 $min^{-1}$ for decarbonylation in either He or $H_2$ are several times larger than those for $Mn_2(CO)_{10}$ alone. These differences may be due to the presence of metallic (zero-valent) Fe which may facilitate decarbonylation of $Mn_2(CO)_{10}$, perhaps by acting as nucleation sites, as proposed for $Fe(CO)_5$ (*71*), or by providing atomic oxygen via CO dissociation on the Fe. This provides indirect evidence that the Fe and Mn phases are in intimate contact because if these two phases are separated, the decarbonylation kinetics for $Mn_2(CO)_{10}$ should be the same.

The adsorption behavior of CO on the decomposed clusters showed that no detectable CO species were present at either 195 K or 300 K on any of the catalysts after LTR. Furthermore, no detectable CO species were observed at 195 K following HTR, but subsequent heating to 300 K in 11 Torr CO in flowing He resulted in the appearance of $Fe(CO)_5$ in all cases. This appearance was most significant for Fe/C, as $Fe_2Mn$/C showed the presence of significantly less $Fe(CO)_5$, which implies that Mn reduces carbonyl formation (*55*). The addition of K to the Fe or Fe–Mn catalysts, however, had a more significant effect as the formation of $Fe(CO)_5$ was greatly reduced. This reduction in carbonyl formation can probably be ascribed to the presence of the much larger Fe particles due to sintering promoted by the potassium. The implication of these results is that $Fe_2Mn$/C catalysts become more iron-like after a HTR step, indicating the presence of some highly dispersed Fe after HTR, which is consistent with MES results (*61*), along with a decrease in the Mn–Fe contact due to phase separation.

The spectra following cooling from reaction conditions, shown in Fig. 22, reveal bands at 2875 and 2960 $cm^{-1}$ due to $CH_3$ species and at 2875 and 2960 $cm^{-1}$ due to $CH_2$ species, and they indicate that the $CH_2/CH_3$ ratio of the adsorbed hydrocarbon species increases going from $Fe_3$/C to $Fe_2Mn$/C to $KFe_3$/C, indicating an increase in chain length. This observation is very reasonable as K is known to increase the chain growth probability (*12*). It is presumed at this time that these reaction products reside primarily on the carbon surface rather than on the iron surface itself (*119, 120*).

## SUMMARY

The genesis of carbon-supported Fe, Fe–Mn, and K-promoted Fe catalysts has been examined using DRIFTS to quantitatively monitor the thermal decomposition of five stoichiometric carbonyl clusters. All decomposition processes were described well by first-order kinetics, and from these results rate constants and activation energies were obtained. The $Mn_2(CO)_{10}$ clusters were most stable, having decarbonylation rate constants near 0.001 $min^{-1}$ at 350 K and high $E_a$ values of 32–37 kcal/mol under either He or $H_2$. The $Fe_3(CO)_{12}$ clusters decomposed most readily, with $k_1$ values around 1 $min^{-1}$ and lower $E_a$ values of 18–21 kcal/mol. $K[HFe_3(CO)_{11}]$, $K[Fe_2Mn(CO)_{12}]$, and $NEt_4[Fe_2Mn(CO)_{12}]$ clusters typically had rate constants between 0.1 and 0.2 $min^{-1}$ and activation energies of 16–19 kcal/mol under either gas; however, both Mn-containing clusters initially decomposed to $Mn_2(CO)_{10}$ and an $[HFe_4(CO)_{13}]^-$ species under $H_2$ before forming the final products. No $Mn_2(CO)_{10}$ formation was observed during either the impregnation step or the decarbonylation of $NEt_4[Fe_2Mn(CO)_{12}]$ under He. Differences in $k_1$ and $E_a$ values for $Mn_2(CO)_{10}$ decomposition

in the presence of iron imply that the reduced Fe particles facilitate this reaction and promote intimate Fe–Mn oxide contact. On the highly dispersed, thoroughly decomposed Fe/C catalysts, $Fe(CO)_5$ was reversibly formed when exposed to CO at 300 K, which indicates the presence of very small reduced Fe particles. The identification of these different Fe phases has been confirmed by Mössbauer spectroscopy in a complementary study (*61*).

After running under reaction conditions for syngas conversion and cooling to 300 K, distinct bands associated with $CH_2$ and $CH_3$ groups could be observed, and these species are presumed to be primarily on the carbon surface, based on previous studies. The increase in the relative concentration of the $CH_2$ group when K is present in the initial cluster is consistent with the well-known effect of K in promoting chain growth. These results demonstrate that the capability now exists to characterize carbon-supported metal catalysts by an IR method, namely DRIFTS.

## ACKNOWLEDGMENTS

This research was supported by the NSF Kinetics and Catalysts Program through Grant CBT-8619619 and by the donors of the Petroleum Research Fund, administered by the American Chemical Society.

## REFERENCES

1. Storch, H. H., Golumbic, N., and Anderson, R. B., "The Fischer–Tropsch and Related Syntheses." Wiley, New York, 1951.
2. Emmett, P. H., "Catalysis," Vol 4. Reinhold, New York, 1956.
3. Kolbel, H., Ralek, M., and Tillmetz, K. D., *13th Int. Soc. Eng. Conv. Soc. Aut. Eng.*, 482 (1982).
4. Schulze, J., *Chem. Ing. Technol.* **46,** 925 (1974).
5. Kolbel, H., and Ralek, M., *Catal. Rev. Sci. Eng.* **21,** 227 (1980).
6. Hu, Y. C., *Hydrocarbon Process.* **5,** 88 (1985).
7. McVicker, G. B., and Vannice, M. A., *J. Catal.* **63,** 25 (1980).
8. Kitzelmann, D., Vielstich, W., and Ditrich, T., *Chem. Ing. Technol.* **49,** 463 (1977).
9. Bussemeier, B., Frohning, C. D., and Cornils, B., *Hydrocarbon Process.* **55,** 101 (1976).
10. Fischer, F., and Tropsch, H., "Gesammelte Abhandlungen zur Kenntris der Kohle," Vol. 10, p. 407. Bontraeger, Berlin, 1932.
11. Kitzelmann, D., and Vielstich, W., "2nd Kolloquim Fischer–Tropsch Synthese, Julich, West Germany, 1978."
12. Van Dijk, W. L., Niemantsverdriet, J. W., Van der Kraan, A. M., and Van der Baan, H. S., *Appl. Catal.* **2,** 273 (1982).
13. Madon, R. J., and Shaw, H., *Catal. Rev. Sci. Eng.* **15,** 69 (1977).
14. Vannice, M. A., Walker, P. L., Jung, H.-J., Moreno-Castilla, C., and Mahajan, O. P., *Proc. 7th Inter. Congress on Catalysis,* p. 460, 1981.
15. Kolbel, H., and Tillmetz, K. D., Belgian Patent 837628.
16. Ralek, M., "2nd Kolloquim Fischer–Tropsch Synthese, Julich, West Germany, 1978."
17. Bub, G., Baerns, M., Bussemeier, B., and Frohning, C., *Chem. Eng. Sci.* **35,** 348 (1980).
18. Copperthwaite, R. G., Hack, H., Hutchings, G. J., and Sellschop, J. P. F., *Surf. Sci.* **164,** L827 (1985).
19. Deckwer, W. D., Lehmann, H. J., Ralek, M., and Schmidt, B., *Chem. Ing. Technol.* **53,** 818 (1981).
20. Egiebor, N. O., and Cooper, W. C., *Appl. Catal.* **14,** 323 (1985).
21. El Deen, A. Z., Jacobs, J., and Baerns, M., *ACS Symp. Ser.* **65,** 26 (1978).
22. Grzybek, T., Papp, H., and Baerns, M., *Appl. Catal.* **29,** 335 (1987).
23. Grzybek, T., Papp, H., and Baerns, M., *Appl. Catal.* **29,** 351 (1987).
24. Huff, G. A., and Satterfield, C. N., *J. Catal.* **85,** 370 (1984).
25. Hughes, S. C., Newman, J. O. H., and Bond, G. C., *Appl. Catal.* **30,** 303 (1987).
26. Hutchings, G. J., and Boeyens, J. C. A., *J. Catal.* **100,** 507 (1986).
27. Jaggi, N. K., Schwartz, L. H., Butt, J. B., Papp, H., and Baerns, M., *Appl. Catal.* **13,** 347 (1985).
28. Jensen, K. B., and Massoth, F. E., *J. Catal.* **92,** 109 (1985).
29. Jensen, K. B., and Massoth, F. E., *J. Catal.* **92,** 98 (1985).
30. Kreitman, K. M., Baerns, M., and Butt, J. B., *J. Catal.* **105,** 319 (1987).
31. Maiti, G. C., Malessa, R., and Baerns, M., *Appl. Catal.* **5,** 151 (1983).
32. Maiti, G. C., Malessa, R., Lochner, U., and Baerns, M., *Appl. Catal.* **9,** 137 (1984).
33. Maiti, G. C., Malessa, R., Lochner, U., Papp, H., and Baerns, M., *Appl. Catal.* **16,** 215 (1985).
34. Lochner, U., Papp, H., and Baerns, M., *Appl. Catal.* **23,** 339 (1986).
35. Lohrengel, G., and Baerns, M., *Ber. Bunsenges. Phys. Chem.* **87,** 335 (1983).
36. Pennline, H. W., Zarochak, M. F., Tischner, R. E., and Schehl, R. R., *Appl. Catal.* **21,** 313 (1986).

37. Podesta, W., Guntzer, W., and Ralek, M., *Chem. Ing. Technol.* **55,** 631 (1983).
38. Satterfield, C. N., and Stenger, H. G., *Ind. Eng. Chem. Process. Des. Dev.* **23,** 26 (1984).
39. Schulz, H., "Proceedings, 5th International Congress on Catalysis, Varna, Bulgaria, Oct. 3–4, 1983."
40. Schulz, H., and Gockebay, H., "9th Conference on Catalysis of Organic Reactions, Charleston, SC, Apr. 1982."
41. Soled, S. L., and Fiato, R. A., U.K. Patent GB 2151500 A, 1985.
42. Stencel, J. M., Diehl, J. R., Miller, S. R., Anderson, R. A., and Zarochak, M. F., *Appl. Catal.* **33,** 129 (1987).
43. Suzdorf, A. R., Bakmutova, N. I., Efremov, A. A., and Kuznetsov, V. L., *React. Kinet. Catal.* **31,** 343 (1986).
44. Benecke, W., Schulz, R., Feller, H. G., and Ralek, M., "Proceedings, 8th International Congress on Catalysis," Vol. 4, p. 219, 1984.
45. Barrault, J., Forquy, C., and Perrichon, V., *Appl. Catal.* **5,** 119 (1983).
46. Barrault, J., and Renard, C., *Appl. Catal.* **14,** 133 (1985).
47. Barrault, J., and Renard, C., *Nouv. J. Chim.* **7,** 149 (1983).
48. Barrault, J., Renard, C., Yu, L. T., and Gal, J., "Proceedings, 8th International Congress on Catalysis," Vol. 2, p. 101, 1984.
49. Abbot, J., Clark, N. J., and Baker, B. G., *Appl. Catal.* **26,** 141 (1986).
50. Bruce, L., Hope, G., and Turney, T. W., *React. Kinet. Catal.* **20,** 175 (1982).
51. Kuznetsov, V. L., Danilyuk, A. F., Kolosova, I. E., and Yermakov, Y. I., *React. Kinet. Catal.* **21,** 249 (1982).
52. Maksimov, Y. V., Matveev, V. V., Shashkin, D. P., Golovina, O. A., and Parshina, A., *Kinet. Catal.* **27,** 798 (1987).
53. Oades, R. D., Morris, S. R., Moyes, R. B., Parkyns, N. D., and Bradshaw, D. I., *Appl. Catal.* **25,** 77 (1986).
54. Sano, T., Yanagisawa, H., Saito, K., Okabe, K., Okado, H., Takaya, H., and Bando, L., *Appl. Catal.* **19,** 247 (1986).
55. Venter, J. J., Kaminsky, M., Geoffroy, G. L., and Vannice, M. A., *J. Catal.* **103,** 450 (1987).
56. Venter, J. J., Kaminsky, M., Geoffroy, G. L., and Vannice, M. A., *J. Catal.* **105,** 155 (1987).
57. Kaminsky, M., Yoon, K. J., Geoffroy, G. L., and Vannice, M. A., *J. Catal.* **91,** 338 (1985).
58. Jung, H. J., Walker, P. L., and Vannice, M. A., *J. Catal.* **75,** 416 (1982).
59. Venter, J. J., and Vannice, M. A., *J. Amer. Chem. Soc.* **109,** 6204 (1987).
60. Venter, J. J., and Vannice, M. A., *Appl. Spectrosc.* **42,** 1096 (1988).
61. Chen, A., Phillips, J., Venter, J. J., and Vannice, M. A., *J. Catal.*, in press.
62. Venter, J. J., Chen, A., Phillips, J., and Vannice, M. A., *J. Catal.*, sub. for pub.
63. Jung, H. J., Vannice, M. A., Mulay, L. N., Stanfield, R. M., and Delgass, W. N., *J. Catal.* **76,** 208 (1982).
64. Anderson, R. B., and Emmett, P. H., *J. Phys. Chem.* **56,** 753 (1952).
65. Ruff, J. K., *Inorg. Chem.* **7,** 1818 (1968).
66. Hodali, H. A., Arcus, C., and Shriver, D. F., *Inorg. Synth.* **20,** 218 (1980).
67. Shriver, D. F., and Drezdon, M. A., "The Manipulation of Air Sensitive Compounds," 2nd ed. Wiley–Interscience, New York, 1986.
68. Venter, J. J., and Vannice, M. A., *J. Amer. Chem. Soc.*, in press; *Inorg. Chem.*, in press.
69. Venter, J. J., and Vannice, M. A., *Carbon* **26,** 889 (1988); Venter, J. J., Ph.D. thesis, Pennsylvania State University, Aug. 1988.
70. Krishnan, K., and Ferraro, J. R., "Fourier Transform Infrared Spectroscopy: Techniques Using Fourier Transform Interferometry," Vol. 3, pp. 149. Academic Press, New York, 1986.
71. Venter, J. J., and Vannice, M. A., *J. Phys. Chem.*, in press.
72. Calderazzo, F., and L'Eplattenier, F., *Inorg. Chem.* **6,** 1220 (1967).
73. Ballivet-Tkatchenko, D., and Coudurier, G., *Inorg. Chem.* **18,** 558 (1979).
74. Haas, H., and Sheline, R. K., *J. Chem. Phys.* **47,** 2996 (1967).
75. Hanson, B. E., Bermeaster, J. J., Petty, J. T., and Connaway, M. C., *Inorg. Chem.* **25,** 3089 (1986).
76. Jones, L. H., McDowell, R. S., Goldblatt, M., and Swanson, B. I., *J. Chem. Phys.* **57,** 2050 (1972).
77. Cataliotti, R., Foffani, A., and Marchetti, L., *Inorg. Chem.* **10,** 1594 (1971).
78. Guglielminotti, E., and Zecchina, A., *J. Mol. Catal.* **24,** 331 (1984).
79. Bigorgne, M., *J. Orgmet. Chem.* **24,** 211 (1970).
80. Shojaie, A., and Atwood, J. D., *Organomet.* **4,** 187 (1985).
81. Farmery, K., Kilner, M., Greatrex, R., and Greenwood, N. N., *J. Chem. Soc. A,* 2339 (1969).
82. Alich, A., Nelson, N. J., Strope, D., and Striver, D. F., *Inorg. Chem.* **11,** 2976 (1972).
83. Edgell, W. F., Huff, J., Thomas, J., Lehman, H., Angell, C., and Asato, G., *J. Amer. Chem. Soc.* **82,** 1254 (1960).
84. Abel, E. W., and Stone, F. G. A., *Q. Rev.* **23,** 325 (1969).
85. Edgell, W. F., Yang, M. T., Bulkin, B. J., Bayer, R., and Koizumi, N., *J. Amer. Chem. Soc.* **87,** 3080 (1965).

86. Fletcher, S. C., Poliakoff, M., and Turner, J. J., *Inorg. Chem.* **25,** 3597 (1986).
87. Kristoff, J. S., and Shriver, D. F., *Inorg. Chem.* **13,** 499 (1974).
88. Lazar, K., Matusek, K., Mink, J., Dobos, S., Guczi, L., Marko, L., and Reiff, W. M., *J. Catal.* **87,** 163 (1984).
89. Catton, F. A., and Wilkinson, G., *J. Amer. Chem. Soc.* **79,** 752 (1957).
90. Sheline, R. K., *J. Amer. Chem. Soc.* **73,** 1615 (1951).
91. Cotton, F. A., and Hunter, D. L., *Inorg. Chim. Acta* **11,** L9 (1974).
92. Hughes, F., Smith, A. K., Ben Taarit, Y., Basset, J. M., and Commereuc, D., *J. Chem. Soc. Chem. Commun.*, 68 (1980).
93. Pierantozzi, R., McQuade, K. J., Gates, B. C., Wolf, M., and Knozinger, H., *J. Amer. Chem. Soc.* **101,** 5436 (1979).
94. Grant, S. M., and Manning, A. R., *Inorg. Chim. Acta* **31,** 41 (1978).
95. Psaro, R., Dossi, C., and Ugo, R., *J. Mol. Catal.* **21,** 331 (1983).
96. Anders, U., and Graham, W. A. G., *J. Chem. Soc. Chem. Commun.*, 291 (1966).
97. Hodali, H. A., Shriver, D. F., and Ammlung, C. A., *J. Amer. Chem. Soc.* **100,** 5239 (1978).
98. Effa, J. B. N., Lieto, J., and Aune, J. P., *Inorg. Chim. Acta* **65,** L105 (1982).
99. Wilkinson, J. R., and Todd, L. J., *J. Orgmet. Chem.* **118,** 199 (1976).
100. Hughes, F., Basset, J. M., Ben Taarit, Y., Choplin, A., Primet, M., and Rojas, L., *J. Amer. Chem. Soc.* **104,** 7020 (1982).
101. Iwamoto, M., Nakamura, S. I., and Kusano, L., *J. Phys. Chem.* **90,** 5244 (1986).
102. Flitcroft, P., Higgins, D. K., and Raesz, H. H., *Inorg. Chem.* **3,** 1123 (1964).
103. Haines, L. I. B., Hopgood, D., and Poe, A. J., *J. Chem. Soc. A*, 420 (1968).
104. Hyhms, I. J., and Lippincott, E. R., *Spectrochim. Acta A* **25,** 1845 (1969).
105. Schubert, E. H., and Sheline, R. K., *Z. Naturforsch. B* **20,** 1306 (1965).
106. King, D. L., *J. Catal.* **61,** 77 (1980).
107. Tipson, R. S., "Infrared Spectroscopy of Carbohydrates," NBS Monograph 110. Natl. Bur. Standards, Washington, DC, 1968.
108. McBreen, P. H., Erley, W., and Ibach, H., *Surf. Sci.* **148,** 292 (1984).
109. Kanai, H., Tan, B. J., and Klabunde, K. J., *Langmuir* **2,** 760 (1986).
110. Klabunde, K. J., and Imizu, Y., *J. Amer. Chem. Soc.* **106,** 2721 (1984); Tan, B. J., Klabunde, K. J., Tanaka, T., Kanai, H., and Yoshida, S., *J. Amer. Chem. Soc.* **110,** 5951 (1988).
111. Wrighton, M. S., Graff, J. L., Luong, J. C., and Reichel, C. L., "Reactivity of Metal–Metal Bonds" (M. H. Chisholm, Ed.). *Amer. Chem. Soc.*, Washington, DC, 1981.
112. Levenson, R. A., Gray, H. B., *J. Amer. Chem. Soc.* **97,** 6042 (1975).
113. Wegman, R. W., Olsen, R. J., Gard, D. R., Faulkner, L. R., and Brown, T. L., *J. Amer. Chem. Soc.* **103,** 6089 (1981).
114. Hughey, J. L., Anderson, C. P., and Meyer, T. J., *J. Organomet. Chem.* **125,** C49 (1977).
115. Waltz, W. L., Hackelberg, O., Dorfman, L. M., and Wojcicki, A., *J. Amer. Chem. Soc.* **100,** 7259 (1978).
116. Candlin, J. P., and Shortland, A. C., *J. Organomet. Chem.* **16,** 289 (1969).
117. Alich, A., Nelson, N. J., Strope, D., and Shriver, D. F., *Inorg. Chem.* **11,** 2976 (1972).
118. Hanson, B. E., Bergmeaster, J. J., Petty, J. T., and Connaway, M. C., *Inorg. Chem.* **25,** 3089 (1986).
119. Ekerdt, J. G., and Bell, A. T., *J. Catal.* **62,** 19 (1980).
120. Ekerdt, J. G., and Bell, A. T., *J. Catal.* **58,** 170 (1979).